Title

Directional excitatory input to direction-selective ganglion cells in the rabbit retina

Journal

The Journal of Comparative Neurology, 527(1)

ISSN

1550-7149

Authors

Percival, Kumiko A
Venkataramani, Sowmya
Smith, Robert G
et al.

Publication Date

2019

DOI

10.1002/cne.24207

Peer reviewed

HHS Public Access

Author manuscript

J Comp Neurol. Author manuscript; available in PMC 2020 January 01.

Published in final edited form as:

J Comp Neurol. 2019 January 01; 527(1): 270–281. doi:10.1002/cne.24207.

Directional excitatory input to direction-selective ganglion cells in the rabbit retina

Kumiko A. Percival[1], **Sowmya Venkataramani**[1], **Robert G. Smith**[2], and **W. Rowland Taylor**[1]

[1]Department of Ophthalmology, Casey Eye Institute, Oregon Health & Science University, Portland, Oregon

[2]Department of Neuroscience, University of Pennsylvania, Philadelphia, Pennsylvania

Abstract

Directional responses in retinal ganglion cells are generated in large part by direction-selective release of γ-aminobutyric acid from starburst amacrine cells onto direction-selective ganglion cells (DSGCs). The excitatory inputs to DSGCs are also widely reported to be direction-selective, however, recent evidence suggests that glutamate release from bipolar cells is not directional, and directional excitation seen in patch-clamp analyses may be an artifact resulting from incomplete voltage control. Here, we test this voltage-clamp-artifact hypothesis in recordings from 62 ON-OFF DSGCs in the rabbit retina. The strength of the directional excitatory signal varies considerably across the sample of cells, but is not correlated with the strength of directional inhibition, as required for a voltage-clamp artifact. These results implicate additional mechanisms in generating directional excitatory inputs to DSGCs.

Keywords

amacrine cells; direction selective; excitation; inhibition; rabbit; retinal ganglion cell; synaptic transmission; voltage clamp; RRID:SCR_000325

1 Introduction

The circuitry that generates the directional responses of direction-selective ganglion cells (DSGCs) in the retina has been studied intensively as a model system for neural computation. DSGCs respond strongly for preferred direction stimuli, and weakly for the stimuli in the opposite, non-preferred, or null direction. There is broad agreement that directional inhibitory inputs represent the major mechanism generating such directional responses (Demb, 2007; Taylor & Vaney, 2003; Vaney, Sivyer, & Taylor, 2012). Previous electrophysiological analyses have also reported directional excitation (Fried, Munch, & Werblin, 2005; Taylor & Vaney, 2002), and it has been assumed that directional signals are generated by a combination of directional inhibition and directional excitation. However, consideration of the electrical properties of ganglion cells has led to the proposal that

Correspondence: William Rowland Taylor, School of Optometry, University of California, Berkeley, Berkeley, CA 94720. wrtaylor@berkeley.edu.

directional excitation may arise from imperfect voltage-control during electrophysiological recordings (Poleg-Polsky & Diamond, 2011; Taylor & Smith, 2012).

Imperfect voltage-clamp would produce directional excitation as follows. Due to decrements in axial current flow along dendritic processes, it is inevitable that the magnitude of synaptic conductances within a dendritic arbor will be underestimated when observed via a patch-electrode at the soma (Koch, Douglas, & Wehmeier, 1990; Major, 1993; Schachter, Oesch, Smith, & Taylor, 2010; Spruston, Jaffe, Williams, & Johnston, 1993; Taylor, Mittman, & Copenhagen, 1996; Williams & Mitchell, 2008). As the total membrane conductance becomes larger the electrotonic space constant of the dendrites shrinks and the amplitudes of distal synaptic inputs recorded by an electrode at the soma become more attenuated (Koch et al., 1990). Since inhibitory input to DSGCs is larger in the null than the preferred direction (Fried, Munch, & Werblin, 2002; Taylor & Vaney, 2002), errors in recording the amplitude of the excitatory inputs will be directional, because excitation will be systematically under-estimated in the null versus the preferred direction. Thus, even if excitatory inputs are symmetric, voltage-clamp errors will produce apparent directional tuning of excitation, with larger excitation measured in the preferred relative to null direction. Importantly for this study, the strength of the directional excitation will be directly related to the strength of directional inhibition, which includes both the Null/Preferred ratio of the inhibition, and the magnitude of the inhibitory conductance. Three recent studies in the mouse retina using imaging techniques indicate that the glutamate release from bipolar cells that produces excitation in DSGCs is not directionally tuned (Chen, Lee, Park, Looger, & Zhou, 2014; Park, Kim, Looger, Demb, & Borghuis, 2014; Yonehara et al., 2013).

The goal of this study was to test the hypothesis that the directional excitation reported previously in DSGCs in the rabbit retina is due to the limitations in the spatial and temporal control of the membrane potential in the dendrites that is inherent to voltage-clamp studies. This hypothesis predicts that the strength of the apparent excitatory directional signal will be highly correlated with the strength of the directional inhibitory signal that is supposed to produce it.

2 Methods

2.1 Tissue preparation and maintenance

Experiments were conducted in accordance with protocols approved by the Institutional Animal Care and Use Committee at OHSU and NIH guidelines. Dark-adapted, pigmented rabbits were surgically anaesthetized and the eyes removed under dim-red illumination. The animal was then killed by anesthetic overdose. All subsequent manipulations were performed under infrared illumination (>900 nm) or under dim red light. The anterior portion of the eye was removed, the eyecup transected just above the visual streak, and the dorsal piece discarded. The retina was dissected from the sclera, and a 5 by 5 mm section of central retina was adhered, photoreceptor-side down, to a nitrocellulose membrane or simply placed onto the base of the recording chamber and held in place with a weighted harp. The recording chamber (~0.5 ml volume) was continually perfused (~2 ml/min) with oxygenated bicarbonate-buffered Ames medium (Ames & Nesbett, 1981), buffered to pH 7.4 at 34–36°C.

2.2 Electrophysiology and light stimulation

Patch electrodes were pulled from borosilicate glass to have a final resistance of 4–8 MΩ. For extracellular recording, the electrodes were filled with Ames medium. For intracellular recording, the electrodes were filled with the following electrolytes: 110 mM Cs-methylsulfonate, 10 mM NaCl, 5 mM Na-HEPES, 1 mM Cs-EGTA, 1 mM Na-ATP, 0.1 mM Na-GTP, and 3mM QX-314. The liquid-junction-potential of 10 mV was subtracted from all voltages during analysis. Ganglion cells with a medium soma diameter (~15 μm) and a crescent-shaped nucleus were targeted as potential DSGCs (Vaney, 1994). The extracellular electrode was applied to the soma under visual control through a small hole in the overlying inner limiting membrane, and a loose patch recording was formed. After establishing that the ganglion cell was a DSGC and determining its preferred direction (see below), the extracellular recording electrode was removed and an intracellular patch-electrode applied to the same cell. During whole cell recordings voltage signals were filtered at 2 kHz through the 4-pole Bessel filter and digitized at 5–10 kHz. Series-resistance compensation was applied to the maximum level compatible with stable recordings. The average series resistance was 10.2 ± 4.3 MΩ and the compensation was set to 68 ± 17% (± *SDs, n* = 62).

Light stimuli, generated on a CRT computer monitor (refresh rate 85 Hz, green phosphor only) or an OLED display (Emagin microdisplay; peak lambda = 519 nm, refresh rate 60 Hz), were focused onto the photoreceptor outer segments through a 10× or 20× Olympus water-immersion objective. The background intensities for the CRT monitor and OLED monitors were measured to be ~10^5 and ~3×10^4 photons/μm^2/s, respectively. The percent stimulus contrast was defined as C=100*(L_{max}−L_{min})/L_{mean}, where L is the stimulus intensity and L_{mean} is the background intensity. C was set between 40 and 80% The standard moving stimulus comprised a light or dark bar, moving along its long axis at 1000 μm/s on the retina. All light stimuli were centered with respect to the tip of the recording electrode, and thus also with the soma of the ganglion cell. The bar's width was 150 μm, and its length was set to achieve a 1 s separation of the leading- and trailing-edge responses. The stimulus area was limited by the aperture of the microscope objective, and covered a circular region 1 mm in diameter for the 20× objective. Since the dendritic extents of DSGCs, which delimit the receptive field (Yang & Masland, 1994), reach a maximum of about 400 μm across in rabbit retina (Vaney, 1994), they were fully contained within the stimulus area. The leading edge of the stimulus bar commenced at one edge of the stimulus area and moved until the trailing edge reached the opposite edge. Thus, both leading and trailing edges of the stimulus traversed whole receptive field of the recorded cell.

2.3 Analysis

The preferred direction of the cells and the strength of the directional tuning were calculated from responses to stimuli in each of 12 stimulus directions evenly spanning 360°. Responses were represented as vectors with the angle representing the direction of stimulus motion, and length equal to the number of action potentials. The preferred direction was obtained from the angle of the resultant vector, calculated from the vector sum of the 12 responses. The directional tuning index (DSI) was calculated as the normalized length of the resultant vector. The DSI can range from 0, when the magnitude of the response is the same in all stimulus directions, to 1, for perfect tuning when a response is produced only for a single

stimulus direction (Taylor & Vaney, 2002). We fit the directional tuning data in Figure 1 with a von Mises distribution. The response, R, as a function of stimulus direction is given by, $R = R_{max}\ e^{(k\cos((x-\mu)\ \pi/180))}/e^{k}$, where R_{max} is the maximum response, μ becomes the preferred direction in degrees, and k is the parameter that accounts for the width of the directional tuning.

Light stimulus activated synaptic conductances were estimated from currents recorded under whole-cell voltage clamp as described previously (Buldyrev, Puthussery, & Taylor, 2012; Venkataramani & Taylor, 2010). Briefly, excitatory and inhibitory conductances were measured from current-voltage (I-V) relations generated every 10 ms for net light-evoked currents measured at nine different holding potentials (2110 mV to 50 mV, 20 mV steps). I-V relations were fitted to the equation, $I = G_{inh}(V - E_{Cl}) + G_{exc}(V - V_{exc})$, where V is the membrane potential, G_{inh} is the inhibitory conductance, G_{exc} is the excitatory conductance, E_{Cl} is the chloride equilibrium potential (−70 mV), and V_{exc} is the excitatory reversal potential (0 mV). E_{Cl} and V_{exc} were fixed, whereas G_{inh} and G_{exc} were allowed to vary during fitting. The I-V relations from ON-OFF DSGCs seldom exhibited nonlinear excitation attributable to the contribution of *N*-methyl-*D*-aspartate (NMDA) receptor activation (Poleg-Polsky & Diamond, 2016). Analysis was performed using custom routines written in Igor Pro (www.wavemetrics.com, RRID:SCR_000325).

2.4 Simulations

The NeuronC simulator generated a compartmental model of the cell using the morphology reconstructed from a confocal stack (Smith, 1992). The electrotonic length of the compartments was set <0.03 lambda to ensure accuracy. The patch-clamp recording electrode was modeled as a series resistor and a capacitor connected to the soma of the model. A fourth order Bessel filter was simulated to reproduce the low-pass filter in the recording system (Stincic, Smith, & Taylor, 2016).

We modeled five morphologies, sampled from the visual streak that represented the variability in the size and degree of asymmetry of the dendritic arbors. Soma diameter ranged from 15 to 21 lm. We calibrated the passive (linear) electrotonic properties of the dendritic arbors by first obtaining estimates of the membrane resistivity (R_m), the internal cytoplasmic resistivity, (R_i), and the specific membrane capacitance (C_m). We also estimated the electrode series resistance (R_s) and the electrode capacitance (C_e). To obtain these estimates, we measured passive charging curves from each cell in response to ±5 mV voltage steps from a holding potential of −70 mV (see Stincic et al, 2016). We then fitted model charging curves to the real charging curves using a Levenberg-Marquardt (LM) least-squares procedure to iteratively adjust the above parameters. Convergence on the best fit required 50–300 model runs (Stincic et al., 2016). The ranges for the best fit, parameter values for the five cells were: R_i = 76–120 Ω cm, R_m = 42,000–83,000 Ω cm^2, C_m = 0.6–0.9 μF/cm^2, and R_s = 9–23 MΩ.

The goal was to estimate the effect that varying levels of inhibitory input had upon the amplitude of excitatory postsynaptic currents (EPSCs) produced by a fixed amount of excitatory synaptic conductance. Excitatory inputs were added as a semi-regular array of bipolar cells (density 3,500/μm^2), where each bipolar cell was simulated as a single

compartment, and made a synapse onto the closest dendrite of the DSGC if it was within a criterion distance (typically ~10 μm). The number of bipolar cells that were synaptically connected to the ON- or OFF-arbors of a DSGC ranged from 54 to 130. Similarly, inhibitory inputs were added as a semi-regular array of single compartments representing amacrine cells (3,500/mm^2).

Synapses were modelled as an exponential release function (3 mV/e-fold change) driving a readily releasable pool of vesicles. Neurotransmitter released from each vesicle activated postsynaptic cation channels defined by a ligand-activated Markov sequential-state machine (Schachter et al., 2010; Smith, 1992; Stincic et al., 2016). The effect of the readily-releasable pool was to create a transient input that decayed over the duration of the stimulus. The synaptic release function included a first-order low-pass filter (2 ms). Each bipolar cell synapse was activated by setting the resting potential slightly above the threshold for synaptic release (−45 mV) to provide an excitatory current to the DSGC. We modeled inhibitory synapses similarly.

Light stimuli were implemented by voltage-clamping the bipolar and amacrine cells according to the temporal pattern of the luminance change at that point in the bipolar/amacrine cell array. The model synaptic conductances were determined from the somatic currents “measured” at the soma while holding the model cell at either the excitatory or inhibitory reversal potential, as is done under standard experimental conditions. The somatic conductances were attenuated by a factor of 3–20 compared with the total conductance applied across the dendritic arbors. Models were run on an array of 3.2 GHz AMD Opteron CPUs interconnected by Gigabit Ethernet, with a total of 200 CPU cores. Simulations of the DSGC model took 20–60 min, depending on the model complexity and duration of simulated time. The simulations were run on the Mosix parallel distributed task system under the Linux operating system. For this project, a total of ~50,000 simulations were performed.

3 Results

This study examines only ON-OFF DSGCs in the rabbit retina. The preferred direction of each unit was determined prior to making patch-recordings, by recording extracellular spikes in response to negative contrast (dark) bars, 1 mm long by 125–150 μm wide, moving at 1 mm/s through the center of the receptive field in 12 directions equally spaced 30° apart. Directional tuning of spike responses for OFF and ON responses, normalized for the preferred direction are shown in Figure 1a. The data set initially comprised 71 cells which sampled approximately equally from the four cardinal axes (Figure 1b, left panel). There was a strong correlation between the preferred directions, for the Off and On dendrites (r^2 = 0.98, Figure 1b), but a weaker correlation for the strength of the directional tuning (DSI) for each dendritic arbor (r^2 = .52, Figure 1c). We eliminated nine cells from this initial sample in which the DSI's for both the OFF and ON responses were not greater than 0.3 (points within the grey region in Figure 1c). For the remainder of the paper, responses were elicited by stimuli moving along the preferred-null axis of each cell.

3.1 Directional tuning of excitation and inhibition in DSGCs

The null hypothesis is that the apparent directional tuning of ON and OFF excitatory inputs to DSGCs is an unavoidable measurement artifact generated by asymmetric voltage-clamp errors produced by directional inhibitory input. To test this hypothesis, we set out to determine whether the strength of directional excitatory signals was correlated with the strength of the directional inhibitory signals. We targeted DSGCs within the visual streak in the rabbit, where the dendritic arbors tend to be smaller than in more peripheral regions. Examples of fluorescently labeled cells shown in Figure 2 demonstrate that the overall dendritic extents were rather similar, which would preclude large differences in the voltage-clamp errors between cells arising from morphological variability.

The excitatory and inhibitory conductances during preferred-null stimulation were estimated from current-responses obtained by repeating the stimulus at each of nine holding potentials to obtain the stimulus-evoked current-voltage (I-V) relations (Figure 3a). Current-voltage relations were generated at 10 ms in tervals before and during the stimulus, and were well described by a sum of linear excitatory and inhibitory conductances (Figure 3b). Although similar results might be obtained with the more commonly used 2-point conductance analysis, which is usually performed by measuring currents at the excitatory and inhibitory reversal potentials, sampling additional voltages provided information about the linearity of the current-voltage relations, which enabled us to detect the presence of NMDA receptor mediated inputs (Lee & Zhou, 2006). The presence of an NMDA mediated input within unclamped dendrites could introduce nonlinear voltage-dependent currents that could exacerbate the effects of voltage-clamp artifacts (Poleg-Polsky & Diamond, 2016), however, the IVs were linear, indicating weak or absent contributions from NMDA receptors (Figure 3b). The analysis was applied to all cells in the sample. For the purposes of comparison, the responses were aligned in time to the peak of the leading edge (OFF) response. The thick colored traces show the average for all 62 cells (Figure 3d,e). As expected for a 1 mm long bar moving at 1 mm/s, the peaks of the leading-edge OFF and trailing-edge ON responses were separated by ~1 s (0.99 ± 0.04 s for preferred OFF excitation in Figure 3d). These results are consistent with previous reports; the inhibition was larger in the null direction, and more importantly, even for DSGCs within the visual streak, which tend to be less extensive (Vaney, 1994), excitation was larger in the preferred relative to the null direction (Figure 3d).

The asymmetry in the excitatory and inhibitory conductances can be seen by plotting the peak conductance for the preferred direction, response against the peak conductance for the null-direction response (Figure 4a). The scatter of the data points confirms a previous analysis (Taylor & Vaney, 2002) showing considerable variability in the magnitudes of the conductances, and the sizes of the directional asymmetries. Similar variability was seen for both the OFF and ON responses. The null hypothesis predicts correlations between the excitatory and inhibitory DS signals. We defined the strength of the excitatory DS signal as the normalized preferred-direction amplitude, $dsiG_{Exc}$ = (preferred direction excitation)/(preferred+null excitation). Conversely, the strength of the inhibitory DS signal was evaluated as, $dsiG_{Inh}$ = (null direction inhibition)/(preferred+null inhibition). Nondirectional inputs will have dsiG=0.5. The magnitude of the voltage-clamp error will depend on the

total conductance active at any time-point, and therefore, to evaluate the potential effects of voltage-clamp errors, it was essential to measure the amplitude of the excitation and inhibition at the same time-points. The data in Figure 4a show the peak excitatory conductance, and the magnitude of the simultaneous inhibition measured at the time of peak excitation. The average $dsiG_{Exc}$ values for the OFF and ON responses were 0.60±0.06 and 0.58±0.05, respectively. These values correspond to peak excitation for the OFF and ON responses being 1.50 and 1.38 times larger in the preferred direction. Conversely, the average OFF and ON $dsiG_{Inh}$ values were 0.85±0.10, and 0.75± 0.10, respectively (n=62, mean±*SD*, Figure 4b). These values correspond to the amplitude of the inhibition for the OFF and ON responses being 5.7 and 3.0 fold larger in the null direction. The null hypothesis predicts a positive correlation between $dsiG_{Exc}$ and dsi-G_{Inh}. The correlation was estimated by linear regression (Figure 4b). The slopes (± *SDs*, n=62) and correlation coefficients for the regression lines were 0.017±0.071, r^2= .087 (OFF), and −0.012±0.071, r^2= .00045 (ON), indicating that the strengths of the excitatory and inhibitory directional signals were weakly correlated for the OFF responses and essentially uncorrelated for the ON responses. This weak or absent correlation is inconsistent with the null-hypothesis, that is, that the directional-difference of the peak excitatory conductance is simply an artifact of voltage-clamp-errors. Presumably other factors must be involved.

The calculated dsiG values normalize the amplitude of the conductance, yet a given $dsiG_{Inh}$ value will induce a larger $dsiG_{Exc}$ for larger amplitude inhibition. Perhaps, the expected positive correlation between $dsiG_{Exc}$ and $dsiG_{Inh}$ is obscured by variability in the amplitudes of the conductance. If this were true, then cells with $dsiG_{Exc}$ close to 0.5 (non-DS excitation), should also have smaller absolute levels of inhibitory input. To test this prediction, we sorted the data into quartiles, according to the magnitudes of $dsiG_{Exc}$ and $dsiG_{Inh}$ for the OFF, and ON responses (Figures 5 and 6). For the sample of 62 cells, the first and third quartiles represent the average of 15 cells and the second and fourth quartiles 16 cells. We sorted the 62 cells according to dsG_{Exc} for the OFF response and averaged the conductance traces for each quartile (Figure 5a). As expected from this procedure, the excitation in the first quartile was very similar in the preferred and null directions ($dsiG_{Exc}$ = 0.52±0.03) and the directional-difference increased fairly linearly across the quartiles, ranging from 0.52 to 0.66 (Figure 5b, black symbols). All possible pair-wise T-tests between quartiles were significantly different ($p < 1.1 \times 10^{-4}$). The $dsiG_{Inh}$ values obtained from the corresponding inhibitory conductance traces in each quartile did not show the consistent increase predicted by the null-hypothesis (Figure 5b, red symbols). Pair-wise T-tests indicated that the second and fourth quartile $dsiG_{Inh}$ values were larger than the first (p=.042 and .034), however, no other comparisons were significant. Moreover, the average magnitude of the null-direction inhibition was constant across the percentile groups (Figure 5c open red circles, pair-wise T-test p ranged from .59 to .99), yet the data indicate that the null-direction excitation became smaller across the quartiles (Figure 5c, open black circles). Pair-wise T-tests indicated that the fourth quartile G_{Exc} value was smaller than the first and second (p = .0066 and .0092), but no other comparisons were significant (p> .063).

The same analysis, sorting instead by the ON excitation, produced similar results (Figure 5d–f). Again, as expected from the sorting procedure the average conductance traces showed systematically larger directional-differences across the quartiles (Figure 5d). The average

dsi-G_{Exc} values ranged from 0.51 to 0.63 (Figure 5e, black symbols). All pair-wise T-tests were significant ($p < .0013$). The corresponding dsi-G_{Inh} values did not show a consistent trend (Figure 5e, red symbols). Similar to the OFF response, the stronger excitatory ON DS signals may have resulted from smaller null-direction excitation (Figure 5f, open black circles). Pair-wise T-tests indicated that the fourth quartile G_{Exc} value was smaller than the second ($p = .046$), however, no others were significant. Similar to the OFF response, there was no systematic change in the null direction inhibition (Figure 5f, open red circles). Together, these data indicate that, contrary to the hypothesis, neither the directional tuning in the inhibitory inputs (dsiG_{Inh}), nor the magnitude of the inhibition, is correlated with the strength of the excitatory DS signal.

We performed a similar analysis on the data, but sorted according to dsiG_{Inh} for the OFF and ON responses, to determine how the amplitude of inhibition varied as dsiG_{Inh} increased. When quartiles were organized according to dsiG_{Inh} for the OFF response, the average inhibitory conductance traces were fairly similar for the null-direction (Figure 6a, blue), while the preferred direction inhibition became systematically smaller across the quartiles (Figure 6a, black). The average dsiG_{Inh} values ranged from 0.71 to 0.97 across the quartiles (Figure 6b, red symbols). All pair-wise T-tests were significant ($p < 6.3 \times 10^{-9}$). The increase in the strength of inhibitory DS across quartiles arises primarily from a decrease in the preferred direction inhibition, while average peaks for the null direction remained steady across quartiles (Figure 6c, red). Note that the directional-differences of the, inhibitory amplitudes in Figure 6c appear larger than might be expected from the amplitudes shown in Figure 6a, because the inhibitory amplitude was measured at the time-point corresponding to the peak of the excitation when the inhibition will influence the size of the excitation (Figures 5a and 6a, vertical broken lines). The average dsiG_{Exc} values ranged from 0.57 to 0.62 across the quartiles (Figure 6b, black). Pair-wise T-tests indicated that the fourth quartile dsiG_{Exc} value was larger than the first ($p = .030$), which is consistent with the null-hypothesis, however, no other comparisons were significant. Similar results were obtained when the data were sorted by the ON inhibitory DS signal (Figure 6d–f), however, there was no significant change in dsiG_{Exc} values across the quartiles. Similar to the analysis for excitation above, these results suggest that voltage-clamp errors may not be the primary factor driving the appearance of directional excitatory signals in voltage-clamp analyses of DSGCs.

A noteworthy outcome of these results is the strong correlation in the strength of the directional signals coming from the OFF and ON dendritic arbors. For example, after sorting according to the peak the OFF excitation, the directional difference of the peak ON excitation was small in the first quartile and increased systematically up to the fourth quartile (Figure 5a). A similar effect is observed for the OFF excitation when the data is ordered according to the ON component (Figure 5d). Moreover, a similar phenomenon can be seen when sorting cells according to the inhibition in Figure 6a,d; the directional-differences for inhibition in the OFF and ON dendritic arbors were correlated. There is considerable variability in the strength of the directional signals in both the OFF and ON dendritic arbors (Figure 4), and a priori one might have expected that sorting the cells according to directional-differences in one arbor might have averaged out directional-

differences across the quartiles for the other. Possible reasons for these correlations are discussed below.

In order to test the hypothesis that voltage-clamp errors were responsible for DS signals, we targeted relatively small DSGCs close to the center of the visual streak. Our rationale was that if voltage-clamp errors were the principal factor, then directional excitation should be weaker in DSGCs within the visual streak, compared with other studies, that did not control as carefully for retinal location (Taylor & Vaney, 2002). On the other hand, since voltage-clamp errors are inevitable in any recording from a distributed dendritic structure, we expected the magnitude of the directional inhibitory and excitatory signals to be correlated. The weak correlation was surprising, and therefore we decided to estimate the expected strength of directional signals produced by voltage-clamp errors, by constructing computer models based on the morphologies of five DSGCs sampled form the visual streak.

For a given morphology (Figure 7a), the passive electrical properties of a model neuron are determined by three parameters, the surface membrane resistivity, R_m (Ω cm^2), the axial resistivity within the processes, R_i (Ω cm), and the membrane capacitance, C_m (μF/cm^2). These parameters were assumed to be isotropic across the dendritic arbors, and were estimated by fitting the models to capacitive current transients produced by ±5 mV 100 ms steps using a least-squares algorithm (see Methods). Excellent agreement between simulated and measured capacitive transients was obtained (compare red and black traces, Figure 7b). To estimate voltage-clamp errors present when recording synaptic inputs via an electrode at the soma, excitatory and inhibitory synapses were distributed across the dendritic arbors for the ON and OFF dendrites. In accord with the null-hypothesis, the excitation applied to the dendrites was identical when simulating inputs in the preferred and null directions. Inhibition was either equal in the preferred and null directions, or was set so that the ratio, null/preferred, became progressively larger. The ratio was increased by increasing the null inhibition, reducing the preferred inhibition, or adjusting both inversely. Simulations were run separately for the OFF and ON dendritic arbors of the five morphologies. The simulations demonstrate the expected inverse relationship between the amplitude of the excitation and inhibition; as inhibition increases, the amplitude of the excitation recorded at the soma decreases (Figure 7c,d), and produces the increase in $dsiG_{Exc}$ seen as $dsiG_{Inh}$ increases (Figure 7e). The variability in the simulation data reflects the different morphologies and the different mixes of synaptic inputs, and mirrors to some extent the real data. The simulations demonstrate that voltage-clamp errors even in relatively small DSGCs can induce directional-differences in the, amplitude of the excitatory inputs that are similar to those produced during physiological stimulation. They also demonstrate that even for small dendritic arbors, voltage-clamp errors ensure that when $dsiG_{Inh} > 0.5$ then $dsiG_{Exc} > 0.5$. The results of these simulations seem inconsistent with the finding that ~25% of the DSGCs in the sample show little evidence of directional excitation, despite large directional-differences in inhibition (Figures 5 and 6). A potential explanation for this apparent anomaly is that starburst amacrine cells (SBACs) release both acetylcholine and γ-aminobutyric acid (GABA). If cholinergic transmission is similar to GABAergic transmission, and is larger in the null relative to the preferred direction, then cholinergic excitation would effectively countermand and thus mask the effects of voltage-clamp errors. To test this hypothesis, we blocked cholinergic excitation with 100 μM hexamethonium chloride (Hex) in three cells,

and a combination of Hex (100μM) and MLA (100μM) in five cells. The results were similar in both groups, and the combined results from the eight cells show that the cholinergic antagonists suppressed OFF and ON preferred-direction excitation to 54 and 51% of control (p = .0029, .0036). A similar degree of suppression was seen for null-direction responses (64%, 63%), however, the effect on the ON response was not significant (OFF, ON, p = .043, .087; Figure 8a). The cholinergic antagonists had no discernible effect on the inhibition for either direction (Figure 8a; but see Fried et al., 2005). We subtracted the excitatory conductance during cholinergic block from the control to estimate the magnitude of the glutamatergic and cholinergic inputs (Figure 8b). Contrary to the hypothesis, the amount of excitatory conductance suppressed by the cholinergic antagonists was not larger during null-direction motion. It is noteworthy that the I-V relations during cholinergic block remained fairly linear (Figure 8c), suggesting that the residual glutamatergic input was not dominated by NMDA receptor activity.

4 Discussion

The results demonstrate that the directional tuning of excitatory inputs to DSGCs in the rabbit retina is weakly correlated with the directional tuning of inhibition (Figures 4–6), which is inconsistent with the notion that directional excitation results entirely from voltage-clamp errors. On the other hand, simulations of voltage-clamp errors in model cells indicate that even in these relatively small dendritic arbors, voltage-clamp errors will contribute significantly to the observed excitatory directional signals (Figure 7). Why are such voltage-clamp effects not consistently observed in the sample of cells? The weak correlation could have been partly due to the large variability in the amplitudes and ratios of the synaptic inputs (Figure 4a; Taylor & Vaney, 2002). We modeled this variability by changing the total inhibition (Pref + Null) and the ratio of the inhibition (Null/Pref) in simulations. While the simulations demonstrate the expected inverse relationship between the amplitudes of excitation and inhibition (Figure 7c), they also suggest that such variability may partly obscure the expected positive correlation relation between $dsiG_{Inh}$ and $dsiG_{Exc}$ (Figure 7e). However, the simulations confirm the expectation that for any directional asymmetry, in the magnitude of the inhibition, voltage-clamp errors will produce an inverse asymmetry in the magnitude of the excitatory conductance when measured by an electrode at the soma. Thus, the simulations cannot account for the cells represented by the first quartile in Figure 5, where there is a large directional-difference in the amplitude of the inhibition, and yet no apparent difference in the excitatory conductance.

A partial solution to this conundrum might be that directional output of acetylcholine offsets the effects of voltage-clamp errors. Along with glutamatergic inputs, DSGCs receive cholinergic excitatory inputs, from SBACs. SBACs are both cholinergic and GABAergic and provide the directional GABAergic input to DSGCs. Calcium transients in SBAC synaptic terminals are stronger for stimuli that move outward from the soma toward the dendritic tips of SBACs than for signals moving inward toward the soma (Euler, Detwiler, & Denk, 2002; Lee, Kim, & Zhou, 2010). The asymmetric calcium signals produce larger GABA release for outward motion parallel with the dendritic branch. These directional inhibitory signals are preserved by selective anatomical connections between each SBAC dendritic branch and underlying DSGCs of the appropriate preferred direction (Briggman, Helmstaedter, & Denk,

2011; Lee & Zhou, 2006; Wei, Hamby, Zhou, & Feller, 2011). Since SBACs are also cholinergic, such connectivity leads to the prediction that the excitatory cholinergic inputs to DSGCs should also be larger in the null-direction than the preferred direction. Such an asymmetry would tend to counter the effects of voltage-clamp errors, and could help explain the current observations. However, paired recordings between SBACs and DSGCs do not reveal this expected asymmetry—inputs from preferred-side and null-side SBACs are equal, at least during step-depolarization of the SBACs (Lee & Zhou, 2006; Pei et al., 2015; Sethuramanujam et al., 2016). Moreover, our experiments demonstrated that blocking cholinergic transmission suppressed excitation without obvious effect on inhibition (Figure 8). There was little evidence for the directional asymmetry described above. The component of the conductance sensitive to the cholinergic blockers, similar to the residual glutamatergic component, was larger in the preferred direction than the null direction. It is interesting to note that, in agreement with a previous study (Fried et al., 2005), stronger directional tuning of inhibition was associated with smaller preferred-direction inhibition rather than enhanced null-direction inhibition (Figure 6c,f), which seems consistent with reciprocal-inhibition models of directional GABA release from SBACs (Ding, Smith, Poleg-Polsky, Diamond, & Briggman, 2016; Lee & Zhou, 2006; Lipin, Taylor, & Smith, 2015; Munch & Werblin, 2006).

We initially discounted the possibility that there is directional release of glutamate from bipolar cell terminals based on three recent studies (Chen et al., 2014; Park et al., 2014; Yonehara et al., 2013). Calcium indicator dyes (GCaMP3) or glutamate-sensing fluorescent reporters (iGluSnFR) were used to monitor the activity of bipolar cells presynaptic to DSGCs. In all three studies, calcium transients within bipolar cell terminals, and extracellular glutamate concentrations near bipolar cell terminals, measured during light stimulation showed no directional biases, suggesting that glutamate release from bipolar cells does not play a role in establishing directional signals in DSGCs. However, the directional difference in the peak excitatory conductance change is brief (~100 ms; Figure 5) relative to the time-resolution of the previous imaging studies. Nonetheless, the time-integral of the electrical measurements should display a similar directional difference as the imaging data. We found that the integrated excitatory conductance was 18 ± 10% larger in the preferred relative to the null direction (mean ± SD, $n = 62$). Such a difference may be difficult to detect in imaging studies that evaluate responses by measuring changes in the amplitudes of fluorescence signals (Chen et al., 2014; Park et al., 2014; Yonehara et al., 2013), particularly given the large variability in the, amplitudes of the synaptic inputs in both rabbit and mouse. Detection of directional excitatory signals using iGluSnFR fluorescence may be fraught with the possibility of contamination from extraneous signals due to transmitter spillover and potential complications arising from re-uptake mechanisms. A recent study found that excitatory inputs to DSGCs remained directional even after the direct inhibitory input to DSGCs was almost eliminated (Pei et al., 2015), which also suggests that directional excitation in DSGCs may not simply result from voltage-clamp errors.

Previous reports have shown that blocking NMDA receptors (NMDARs) suppresses spiking in DSGCs (Kittila & Massey, 1997; Tjepkes & Amthor, 2000; Weng, Sun, & He, 2005). Two recent studies have proposed a major role for NMDAR activity in generating directional responses in the mouse retina (Poleg-Polsky & Diamond, 2016; Sethuramanujam et al.,

2016). Moreover, NMDAR mediated excitatory inputs have been observed in rabbit DSGCs (Lee et al., 2010). In other ganglion cell types recorded under identical or very similar recording conditions, nonlinearity in the I-V relations due to NMDARs could be observed, and showed sensitivity to NMDAR antagonists (Lee et al., 2010; Stafford, Manookin, Singer, & Demb, 2014; Venkataramani & Taylor, 2010, 2016). In the current experiments, the I-V relations did not display a strong NMDAR nonlinearity, even after acetylcholine receptors were blocked (Figure 8c), suggesting that any NMDAR mediated component is relatively minor. The reasons for the smaller apparent NMDAR-mediated input relative to other reports are unclear, but may relate to stimulus or adaptation conditions, or perhaps the age of the animals (Lee et al., 2010 used 17–45 day-old rabbits, younger than those used in the present work, which were >90 days old). Precise estimation of the magnitude of any NMDAR component under our recording conditions would require a more detailed analysis.

An interesting feature of the results is the strong correlation between the strength of the directional tuning in the ON and OFF dendritic arbors. For example, the excitatory ON inputs show strong directional tuning when the data are sorted according to the directional tuning for the OFF inputs and vice versa (Figures 5a–c and 6a–c). Such a correlation points to a common mechanism, and in this context the recent finding that a bi-stratified glutamatergic amacrine cell is motion-sensitive and contributes excitatory inputs to DSGCs may be pertinent (Kim, Soto, & Kerschensteiner, 2015; Lee et al., 2014). On the other hand, there also appear to be distinct differences in the circuitry between the ON and OFF arbors (Chen, Pei, Koren, & Wei, 2016; Ishii & Kaneda, 2014). Overall, the results presented here raise more questions than they resolve, and indicate that further work will be required to completely account for directional excitatory signaling observed in DSGCs.

Acknowledgments

This research was supported by NIH grants R01 EY022070, P30 EY010572, and P30 NS061800, by unrestricted departmental funding from Research to Prevent Blindness (New York, NY), and a Sir Keith Murdoch Fellowship, American Australian Association (KAP).

Funding information: NIH, Grant/Award Numbers: R01 EY022070, P30 EY010572, and P30 NS061800; Research to Prevent Blindness (New York, NY); Sir Keith Murdoch Fellowship (KAP), American Australian Association

References

Ames A, Nesbett FB. 1981; In vitro retina as an experimental model of the central nervous system. Journal of Neurochemistry. 37:867–877. [PubMed: 7320727]

Briggman KL, Helmstaedter M, Denk W. 2011; Wiring specificity in the direction-selectivity circuit of the retina. Nature. 471:183–188. [PubMed: 21390125]

Buldyrev I, Puthussery T, Taylor WR. 2012; Synaptic pathways that shape the excitatory drive in an OFF retinal ganglion cell. Journal of Neurophysiology. 107:1795–1807. [PubMed: 22205648]

Chen M, Lee S, Park SJH, Looger LL, Zhou ZJ. 2014; Receptive field properties of bipolar cell axon terminals in the direction-selective sublaminas of the mouse retina. Journal of Neurophysiology. 112:1950–1962. [PubMed: 25031256]

Chen Q, Pei Z, Koren D, Wei W. 2016; Stimulus-dependent recruitment of lateral inhibition underlies retinal direction selectivity. Elife. 5:e21053. [PubMed: 27929372]

Demb JB. 2007; Cellular mechanisms for direction selectivity in the retina. Neuron. 55:179–186. [PubMed: 17640521]

Ding H, Smith RG, Poleg-Polsky A, Diamond JS, Briggman KL. 2016; Species-specific wiring for direction selectivity in the mammalian retina. Nature. 535:105–110. [PubMed: 27350241]

Euler T, Detwiler PB, Denk W. 2002; Directionally selective calcium signals in dendrites of starburst amacrine cells. Nature. 418:845–852. [PubMed: 12192402]

Fried SI, Munch TA, Werblin FS. 2002; Mechanisms and circuitry underlying directional selectivity in the retina. Nature. 420:411–414. [PubMed: 12459782]

Fried SI, Munch TA, Werblin FS. 2005; Directional selectivity is formed at multiple levels by laterally offset inhibition in the rabbit retina. Neuron. 46:117–127. [PubMed: 15820698]

Ishii T, Kaneda M. 2014; ON-pathway-dominant glycinergic regulation of cholinergic amacrine cells in the mouse retina. The Journal of Physiology. 592:4235–4245. [PubMed: 25085888]

Kim T, Soto F, Kerschensteiner D. 2015; An excitatory amacrine cell detects object motion and provides feature-selective input to ganglion cells in the mouse retina. Elife. 4:e08025.

Kittila CA, Massey SC. 1997; Pharmacology of directionally selective ganglion cells in the rabbit retina. Journal of Neurophysiology. 77:675–689. [PubMed: 9065840]

Koch C, Douglas R, Wehmeier U. 1990; Visibility of synaptically induced conductance changes: Theory and simulations of anatomically characterized cortical pyramidal cells. Journal of Neuroscience. 10:1728–1744. [PubMed: 2355247]

Lee S, Chen L, Chen M, Ye M, Seal RP, Zhou ZJ. 2014; An unconventional glutamatergic circuit in the retina formed by vGluT3 amacrine cells. Neuron. 84:708–715. [PubMed: 25456497]

Lee S, Kim K, Zhou ZJ. 2010; Role of ACh-GABA cotransmission in detecting image motion and motion direction. Neuron. 68:1159–1172. [PubMed: 21172616]

Lee S, Zhou ZJ. 2006; The synaptic mechanism of direction selectivity in distal processes of starburst amacrine cells. Neuron. 51:787–799. [PubMed: 16982423]

Lipin MY, Taylor WR, Smith RG. 2015; Inhibitory input to the direction-selective ganglion cell is saturated at low contrast. Journal of Neurophysiology. 114:927–941. [PubMed: 26063782]

Major G. 1993; Solutions for transients in arbitrarily branching cables: III. Voltage clamp problems. Biophysical Journal. 65:469–491. [PubMed: 8369450]

Munch TA, Werblin FS. 2006; Symmetric interactions within a homogeneous starburst cell network can lead to robust asymmetries in dendrites of starburst amacrine cells. Journal of Neurophysiology. 96:471–477. [PubMed: 16598066]

Park SJH, Kim IJ, Looger LL, Demb JB, Borghuis BG. 2014; Excitatory synaptic inputs to mouse on-off direction-selective retinal ganglion cells lack direction tuning. Journal of Neuroscience. 34:3976–3981. [PubMed: 24623775]

Pei Z, Chen Q, Koren D, Giammarinaro B, Acaron Ledesma H, Wei W. 2015; Conditional knock-out of vesicular GABA transporter gene from starburst amacrine cells reveals the contributions of multiple synaptic mechanisms underlying direction selectivity in the retina. Journal of Neuroscience. 35:13219–13232. [PubMed: 26400950]

Poleg-Polsky A, Diamond JS. 2011; Imperfect space clamp permits electrotonic interactions between inhibitory and excitatory synaptic conductances, distorting voltage clamp recordings. PLoS One. 6:e19463. [PubMed: 21559357]

Poleg-Polsky A, Diamond JS. 2016; NMDA receptors multiplicatively scale visual signals and enhance directional motion discrimination in retinal ganglion cells. Neuron. 89:1277–1290. [PubMed: 26948896]

Schachter MJ, Oesch N, Smith RG, Taylor WR. 2010; Dendritic spikes amplify the synaptic signal to enhance detection of motion in a simulation of the direction-selective ganglion cell. PLoS Computational Biology. 6:e1000899. [PubMed: 20808894]

Sethuramanujam S, McLaughlin AJ, DeRosenroll G, Hoggarth A, Schwab DJ, Awatramani GB. 2016; A central role for mixed acetylcholine/GABA transmission in direction coding in the retina. Neuron. 90:1243–1256. [PubMed: 27238865]

Smith RG. 1992; NeuronC: A computational language for investigating functional architecture of neural circuits. Journal of Neuroscience Methods. 43:83–108. [PubMed: 1405746]

Spruston N, Jaffe DB, Williams SH, Johnston D. 1993; Voltage-and space-clamp errors associated with the measurement of electro-tonically remote synaptic events. Journal of Neurophysiology. 70:781–802. [PubMed: 8410172]

Stafford BK, Manookin MB, Singer JH, Demb JB. 2014; NMDA and AMPA receptors contribute similarly to temporal processing in mammalian retinal ganglion cells. The Journal of Physiology. 592:4877–4889. [PubMed: 25217374]

Stincic T, Smith RGRG, Taylor WRR. 2016; Time course of EPSCs in ON-type starburst amacrine cells is independent of dendritic location. The Journal of Physiology. 594:5685–5694. [PubMed: 27219620]

Taylor WR, Mittman S, Copenhagen DR. 1996; Passive electrical cable properties and synaptic excitation of tiger salamander retinal ganglion cells. Visual Neuroscience. 13:979–990. [PubMed: 8903038]

Taylor WR, Smith RG. 2012; The role of starburst amacrine cells in visual signal processing. Visual Neuroscience. 29:73–81. [PubMed: 22310373]

Taylor WR, Vaney DI. 2002; Diverse synaptic mechanisms generate direction selectivity in the rabbit retina. Journal of Neuroscience. 22:7712–7720. [PubMed: 12196594]

Taylor WR, Vaney DI. 2003; New directions in retinal research. Trends in Neurosciences. 26:379–385. [PubMed: 12850434]

Tjepkes DS, Amthor FR. 2000; The role of NMDA channels in rabbit retinal directional selectivity. Visual Neuroscience. 17:291–302. [PubMed: 10824683]

Vaney DI. 1994; Territorial organization of direction-selective ganglion cells in rabbit retina. Journal of Neuroscience. 14:6301–6316. [PubMed: 7965037]

Vaney DI, Sivyer B, Taylor WR. 2012; Direction selectivity in the retina: Symmetry and asymmetry in structure and function. Nature Reviews Neuroscience. 13:194–208. [PubMed: 22314444]

Venkataramani S, Taylor WR. 2010; Orientation selectivity in rabbit retinal ganglion cells is mediated by presynaptic inhibition. Journal of Neuroscience. 30:15664–15676. [PubMed: 21084622]

Venkataramani S, Taylor WR. 2016; Synaptic mechanisms generating orientation selectivity in the ON pathway of the rabbit retina. Journal of Neuroscience. 36:3336–3349. [PubMed: 26985041]

Wei W, Hamby AM, Zhou K, Feller MB. 2011; Development of asymmetric inhibition underlying direction selectivity in the retina. Nature. 469:402–406. [PubMed: 21131947]

Weng S, Sun W, He S. 2005; Identification of ON-OFF direction-selective ganglion cells in the mouse retina. The Journal of Physiology. 562:915–923. [PubMed: 15564281]

Williams SR, Mitchell SJ. 2008; Direct measurement of somatic voltage clamp errors in central neurons. Nature Neuroscience. 11:790–798. [PubMed: 18552844]

Yang G, Masland RH. 1994; Receptive fields and dendritic structure of directionally selective retinal ganglion cells. Journal of Neuroscience. 14:5267–5280. [PubMed: 8083735]

Yonehara K, Farrow K, Ghanem A, Hillier D, Balint K, Teixeira M, et al. Roska B. 2013; The first stage of cardinal direction selectivity is localized to the dendrites of retinal ganglion cells. Neuron. 79:1078–1085. [PubMed: 23973208]

Abbreviations

ATP	adenosine 5′-triphosphate
DSGC	direction selective ganglion cell
EGTA	ethylene glycol-bis(2-aminoethylether)-N,N,N′,N′-tetraacetic acid
GABA	γ-aminobutyric acid
GTP	guanosine 5′-triphosphate
HEPES	4-(2-Hydroxyethyl)piperazine-1-ethanesulfonic acid
MLA	N,2,3,3-Tetramethylbicyclo[2.2.1]heptan-2-amine hydrochloride
QX-314	N-(2,6-Dimethylphenylcarbamoylmethyl)triethylammonium chloride

SBAC	starburst amacrine cell

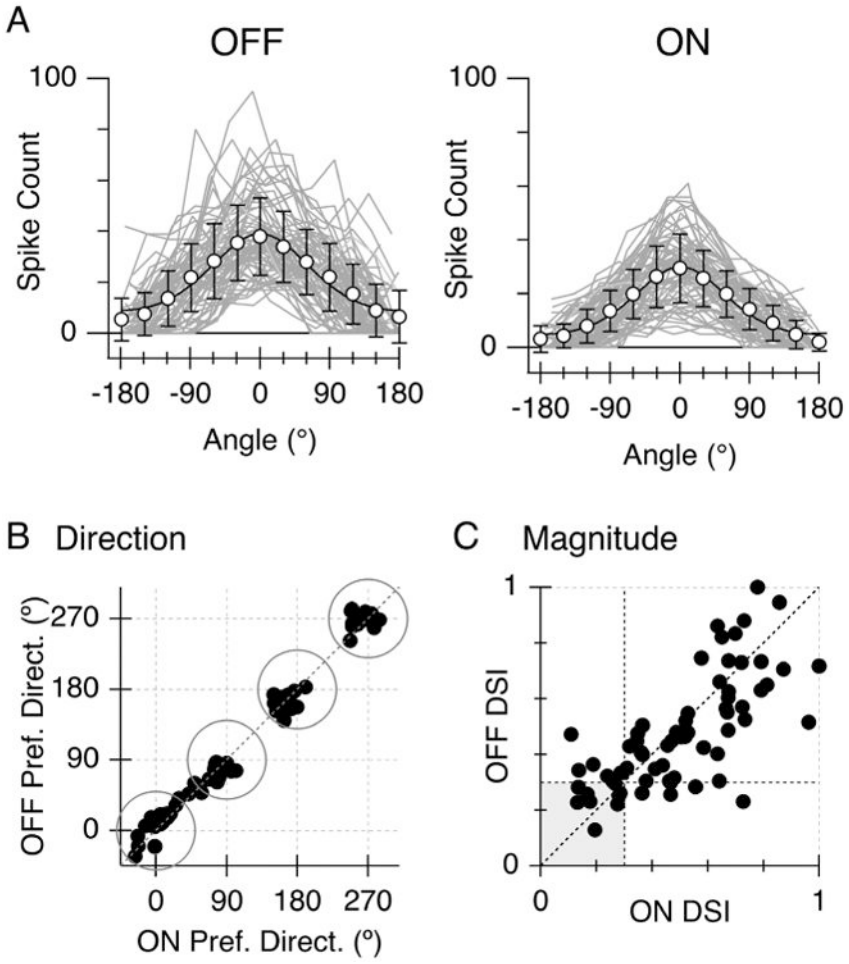

Figure 1.

Directional tuning of ON-OFF direction selective ganglion cells (DSGCs). (a) Spike counts for OFF and ON responses across 12 stimulus directions tested. Angles tested have been normalized to the preferred direction of each DSGC. (b) Preferred directions for ON and OFF responses for each ON-OFF DSGC form four clusters representing the four subtypes tuned to 0°, 90°, 180°, and 270°. (c) Magnitude of spiking plotted for ON responses against OFF responses. Cells in the grey region where either the ON or OFF DSI < 0.3 were omitted from further analysis

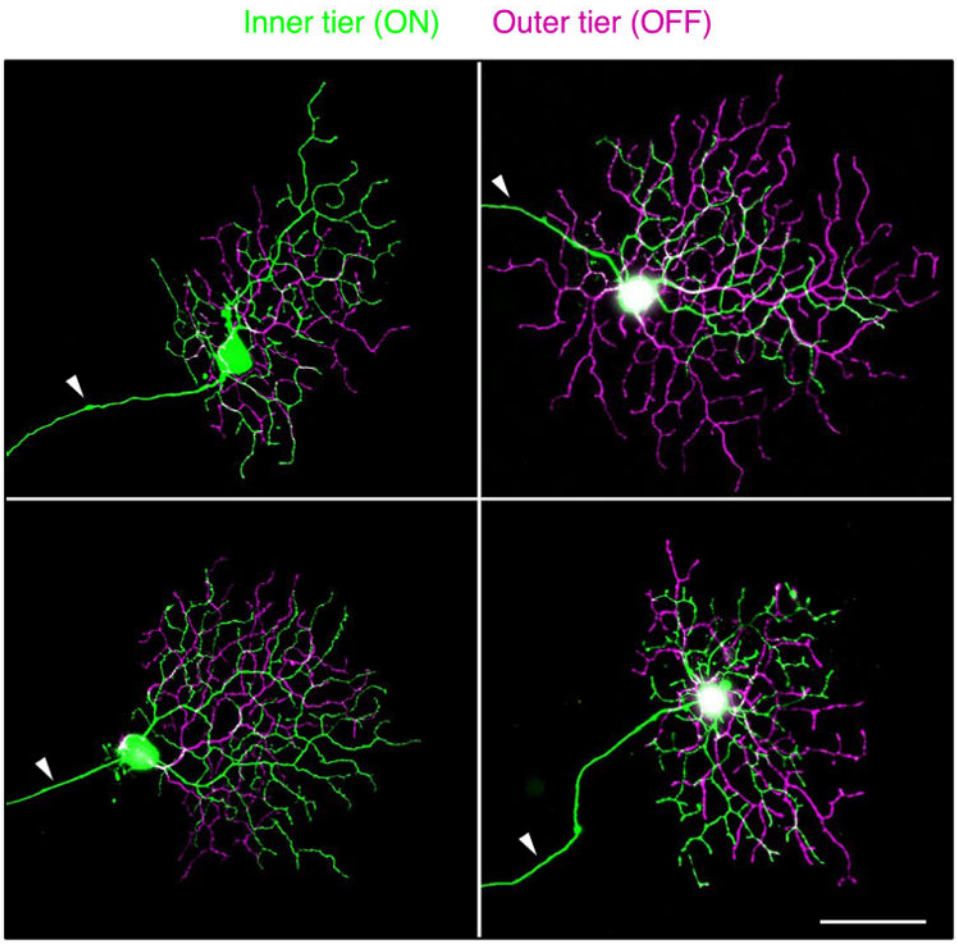

Figure 2.
Morphologies of cells in the visual streak of the rabbit illustrating the extents of the dendritic arbors. Arrowheads indicate the axons. Scale bar = 50 μm

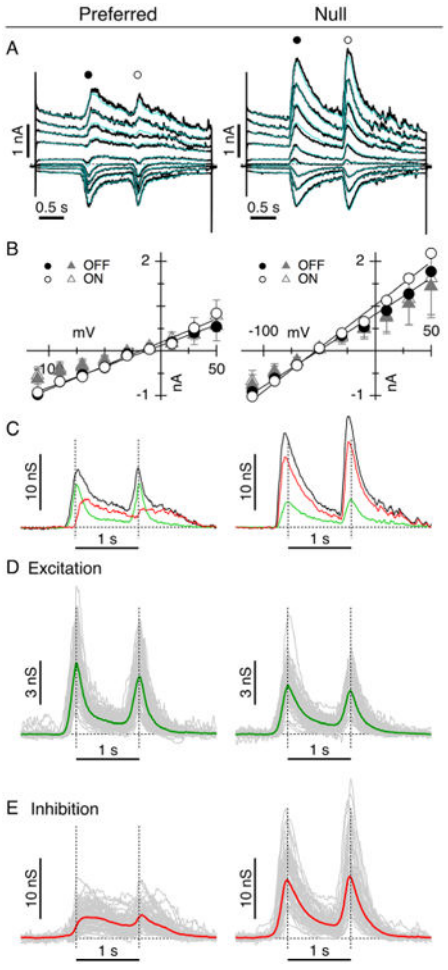

Figure 3.

Measurement of synaptic conductances. (a) Membrane currents in a single DSGC during a series of depolarizing voltage-steps from −110 to +45 mV. The light stimulus comprised a dark bar 150 μm wide by 1 mm long, moving at 1 mm/s parallel to the long axis along the preferred-null axis. The leading (OFF) and trailing (ON) edge responses are well separated as evident by the distinct the peaks in the current traces. Cyan lines show currents calculated from a linear combination of the fitted excitatory and inhibitory conductances shown in (c). (b) Current-voltage (I-V) relations measured at the time-points shown in (a). The excitatory and inhibitory synaptic components were calculated from the linear fits (solid lines) to I-Vs at each time point. The grey data-points show the average I-V relations for the 62 cells analyzed. (c) Total conductance obtained from the slope of the I-V relations in (b) (black trace). I-V relations were measured at 10 ms intervals. The component excitatory and inhibitory conductances are shown in green and red, respectively. (d, e) Excitatory and inhibitory conductances for preferred and null stimulation, estimated from 62 DSGCs. The grey lines show individual cells, and the green and red traces show the averages of all the cells

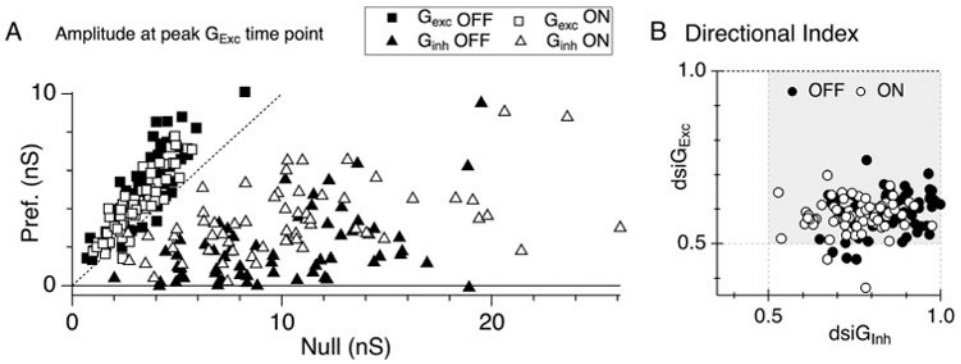

Figure 4.

Conductance amplitude and DSI. (a) Amplitude of the conductance for preferred direction plotted against the amplitude for the null-direction. Amplitudes were measured at fixed time-points corresponding to the peak excitation for the OFF and ON responses in each direction. The dotted line shows the expectation if the magnitudes of the synaptic inputs were independent of stimulus direction. (b) Strength of directional signals for excitation and inhibition. The $dsiG_{Exc}$ is the preferred-excitation as a fraction of the total (Pref + Null) excitation. Similarly, $dsiG_{Inh}$ is the null-inhibition as a fraction of the total (Pref + Null) inhibition

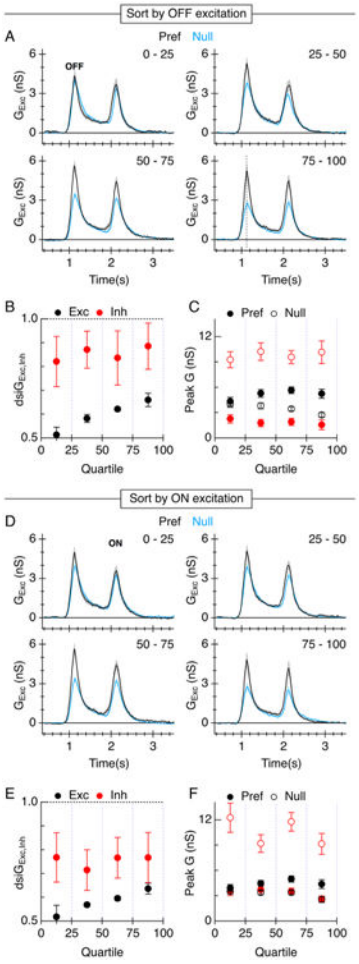

Figure 5.

The strength of the excitatory directional difference is not correlated with the strength of the inhibitory directional difference. Data are from the 62 DSGCs shown in Figure 4. The 62 cells were sorted into quartiles, according to the magnitude of $dsiG_{Exc}$ for the OFF (a–c) or ON (d–f) responses. The first to the fourth quartiles contain 15, 16, 15, and 16 cells, respectively. (a, d) The traces show the average excitatory conductance for each quartile in each stimulus direction, preferred in black, null in blue. (b, e) $dsiG_{Exc}$ and $dsiG_{Inh}$ plotted for each quartile. (c, f) Amplitude of the excitatory conductances (black) measured at the peak (see vertical lines Figure 3d). The amplitude of the inhibitory conductance (red) was measured at the same time-point (see vertical lines Figure 3e)

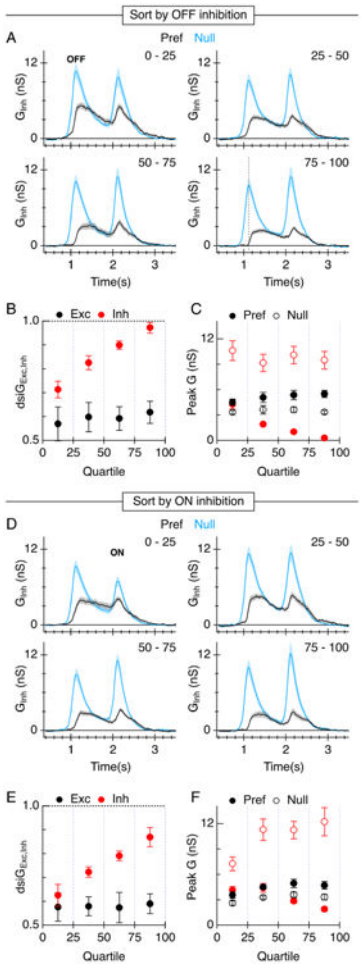

Figure 6.

The strength of the inhibitory directional signal does not predict the strength of the excitatory tuning. The analysis and figure layout are identical to Figure 5, except that the 62 cells were sorted into quartiles, according to the magnitudes of $dsiG_{Inh}$ for the OFF (a–c) or ON (d–f) responses

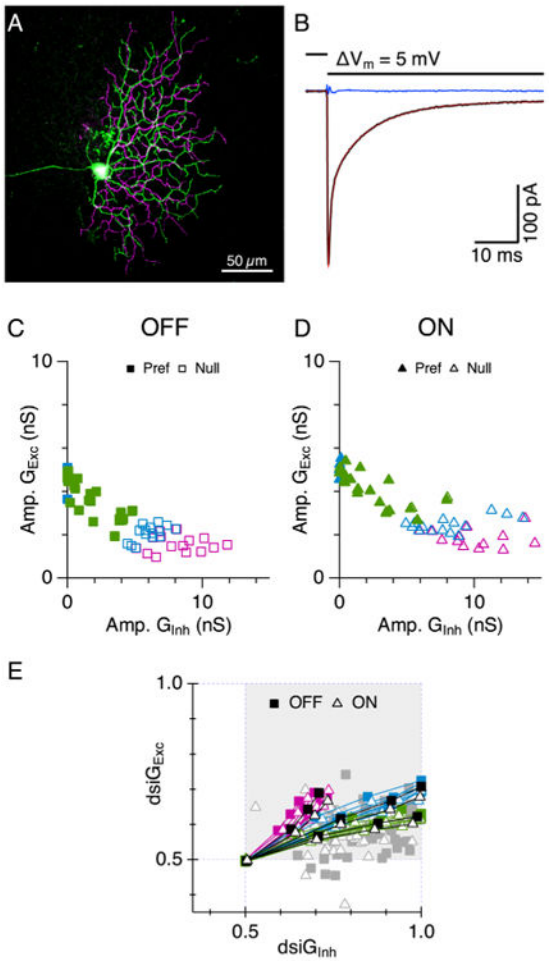

Figure 7.

Simulations of directional response in ON-OFF DSGCs. (a) One of the five morphologies used to generate the models. (b) Capacitive currents obtained from the cell shown in (a) during 5mV voltage-steps from a holding potential of −70 mV. The red overlay shows the fitted current obtained from simulations, which were used to calibrate the electrotonic properties of each model cell. The blue line shows the difference between the simulation and the real data. (c, d) Amplitudes of excitatory (G_{Exc}) conductance plotted against the amplitudes of the inhibitory (G_{Inh}) conductances sampled by a voltage-clamp electrode at the soma of the model. Excitation was fixed at the same constant value for Pref and Null simulations. The inhibitory directional-input was varied in three ways; Inhibition was progressively increased (green) in the Null-direction, or it was decreased in the Pref-direction (magenta), or it was changed in both directions (blue). (e) $dsiG_{Exc}$ and $dsiG_{Inh}$ plotted for the stimulations shown in (c, d). The grey symbols show data replotted from Figure 4c. The solid lines connect simulation results obtained in the same model cell with increasing Null/Pref inhibitory ratios. The black points show the results for the cell in (a). In each case, an initial simulation was performed with symmetric inhibition (data points at 0.5 $dsiG_{Inh}$). Note that in each case, as $dsiG_{Inh}$ increases voltage-clamp errors induce an increase in $dsiG_{Exc}$

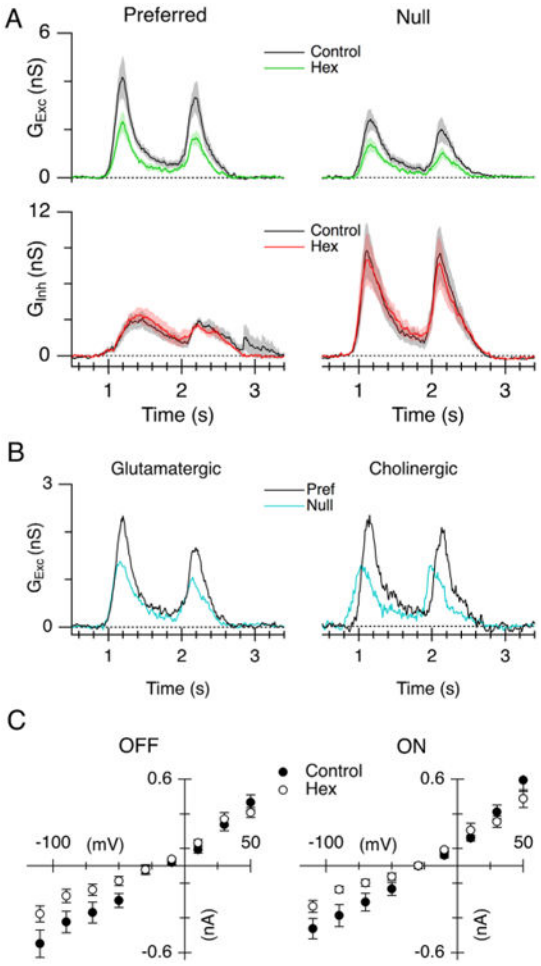

Figure 8.

Effects of blocking cholinergic transmission in the retina. (a) Average excitatory and inhibitory conductances recorded in eight cells before and during cholinergic block with either 100 mM Hex (three cells) or 100 μM Hex + 100 μM MLA (five cells). (b) Difference excitatory conductances. “Glutamatergic” was recorded during cholinergic block (replotted green traces from (a)), and “Cholinergic” was obtained by subtracting the glutamatergic component from the control. (c) Average current-voltage relations for preferred direction stimulation in control (black) and during cholinergic block (open)